Journal of Nuclear Materials 385 (2009) 103–107

Contents lists available at ScienceDirect

Journal of Nuclear Materials

journal homepage: www.elsevier.com/locate/jnucmat

Effective thermal conductivity of MOX raw powder

Kentaro Takeuchi [a,*], Masato Kato [a], Takeo Sunaoshi [b], Shigenori Aono [a], Motoaki Kashimura [a]

[a] Nuclear Fuel Cycle Engineering Laboratories, Japan Atomic Energy Agency, 4-33 Tokai-mura, Naka-gun, Ibaraki 319-1194, Japan
[b] Inspection Development Company, 4-33 Tokai-mura, Naka-gun, Ibaraki 319-1194, Japan

A B S T R A C T

The radial temperature distribution of plutonium and uranium mixed oxide powder loaded into a cylindrical vessel was measured in air and argon gas, and the effective thermal conductivity was calculated from the measured temperature distribution and the decay heat. The effective thermal conductivities were small values of 0.061–0.13 W m^{-1} K^{-1} at about 318 K, and changed significantly with O/M, bulk density and atmospheric gas. The results in this work were analyzed by the model of Hamilton and Crosser and a new model for the effective thermal conductivity of the powder was derived as functions of powder properties and thermal conductivity of atmospheric gas.

1. Introduction

Japan Atomic Energy Agency has fabricated plutonium and uranium mixed oxide (MOX) fuels with about 20% and 30%Pu for a fast breeder reactor (FBR) using MOX raw powder. In the conversion process, Pu content of MOX raw powder is adjusted to about 50% in the solution mixing step of plutonium nitrate and uranyl nitrate, and the powder was prepared by the microwave heating direct denitration method (MH-MOX powder). In the MOX raw powder, Pu causes self heat generation by alpha decay, and the powder temperature increases. In a commercial scale MOX fuel fabrication plant, a special concern is the increase of temperature of MOX raw powder with increasing powder lot size. In addition, another concern is the larger temperature increase caused by the increased amounts of Pu-238 and minor actinides (MAs) which occur with increasing burn-up and recycling of MAs, respectively. The generated heat of MH-MOX raw powder causes an increase in oxygen-to-metal ratio (O/M) by oxidation of powder in the air, degrades additives and overheats equipment [1]. For these reasons, it is essential to control the temperature of the MOX raw powder and to obtain accurate effective thermal conductivity of MOX raw powder for fabrication equipment design. However, the effective thermal conductivity of MOX raw powder has been few reported [2].

The effective thermal conductivity of MOX raw powder is considered as the thermal conductivity of the binary phases which consist of dispersed particles and gas. The thermal conductivity of binary phases has been reported in various phase combination (such as solid–solid, solid–liquid, solid–gas). Particularly, in the solid–solid phase, a number of tests have been carried out to investigate the thermal conductivity of composite material [3–6]. Maxwell [3] investigated the thermal conductivity of the binary phases with dispersed spherical particles. The thermal conductivity of the binary phases with dispersed non-spherical particles has been measured by Fricke [4], Johnson [5], Hamilton and Crosser [6] as a function of particle shapes. In particular, the model of Hamilton and Crosser [6] considers the effects of particle shapes and includes terms for mean particle size and specific surface area.

In the present work, the effective thermal conductivity of MOX raw powder was deduced from the measurement results of the temperature distribution as functions of atmospheric gas and powder properties (such as O/M, bulk density, specific surface area, and mean particle diameter) and analyzed by the model of Hamilton and Crosser.

2. Experimental

2.1. Sample preparation

MOX raw powder which was prepared by the microwave heating direct denitration method was used as sample powder. Sample I and II were obtained by changing the denotation conditions which were controlled by heating power of microwave. Then sample II were heated at 1023 K for 4 h in Ar–5%H_2 (sample III) and air (sample IV) to change O/M, specific surface area, and mean particle size as sample III and IV. Heat treatment conditions and sample powder properties are summarized in Table 1.

2.2. Measurement procedure

A schematic drawing of the temperature measuring equipment is shown in Fig. 1. The equipment had a copper cylinder and

* Corresponding author. Tel.: +81 29 282 1111; fax: +81 29 282 9473.
E-mail address: takeuchi.kentaro@jaea.go.jp (K. Takeuchi).

0022-3115/$ - see front matter © 2008 Elsevier B.V. All rights reserved.
doi:10.1016/j.jnucmat.2008.09.033

Table 1
Heat treatment conditions and powder properties.

Sample	Heat treatment conditions	Pu content[a] (%)	U content[a] (%)	O/M ratio	Specific surface area (m^2/g)	Mean particle size (μm)	Decay heat rate (W/gMOX)
I	–	41.477	43.868	2.03	2.52	0.631	5.51×10^{-3}
II	–	40.029	43.761	2.28	4.33	0.531	6.42×10^{-3}
III	1023 K, Ar–5%H_2	40.825	44.631	2.05	3.73	0.551	6.55×10^{-3}
IV	1023 K, air	40.311	44.069	2.28	3.36	0.716	6.46×10^{-3}

[a] Metal/Oxide.

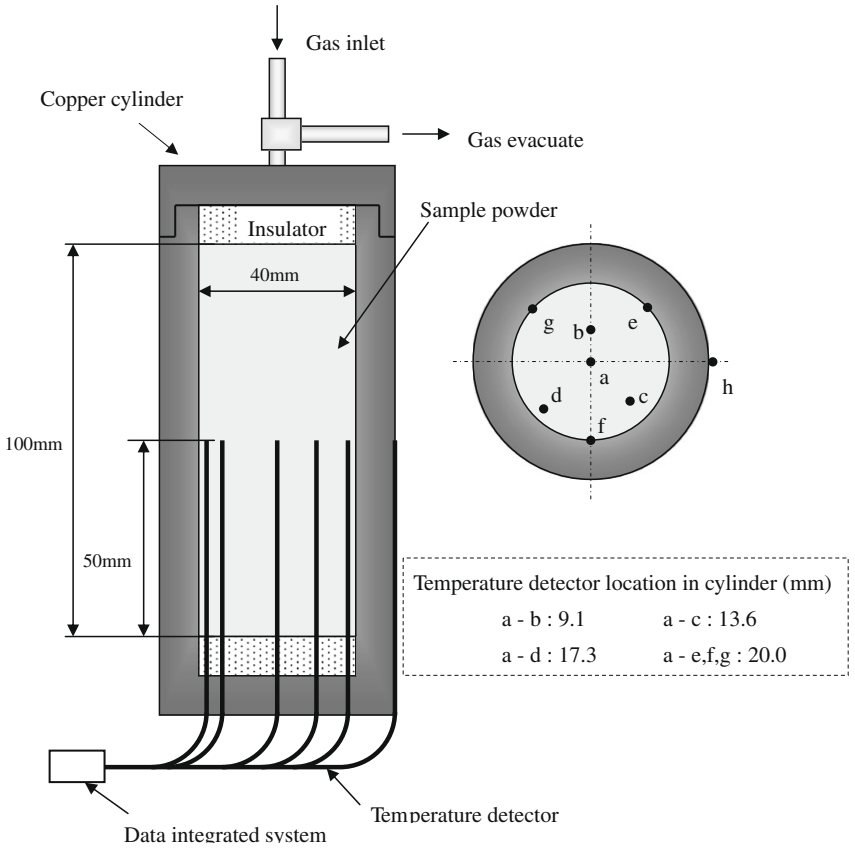

Fig. 1. Schematic of measuring equipment.

insulator, and heat loss in axial direction was less than that in the radial direction. Temperature measurement was done with a platinum resistance temperature detector (Pt-RTD; measurement accuracy ±0.01 K). The temperature detectors were placed at the positions a–h as shown in Fig. 1.

The copper cylinder was filled with MOX raw powder, and the bulk density was controlled by tapping. In some tests, the air was evacuated from the cylinder, which was then filled with argon (Ar). Temperatures were measured by each detector until they became constant. After the temperature measurements, bulk density of MOX raw powder was calculated from the weight and filling volume of sample powder.

2.3. Calculation procedure for effective thermal conductivity

In case of homogeneous heat generation in a cylinder model, the radial temperature distribution is given by

$$t(r) = t_0 + \frac{q}{4\lambda_e}(R^2 - r^2) \quad (1)$$

where $t(r)$ is the temperature at each measurement point, t_0 is cylinder surface temperature, q is heat rate and λ_e is effective thermal conductivity, R is cylinder internal radius and r is distance from the center of the cylinder. The effective thermal conductivity was calculated from the measured temperature distribution and heat rate which was calculated from isotopic composition, calorific value of each isotope [7] and bulk density, by using Eq. (1) assuming that λ_e was constant in the region of the measuring temperatures which was an average temperature of 318 K.

3. Results

The temperatures of the powders loaded into the measuring equipment were measured as parameters of bulk density and kinds of atmospheric gas. An example of the radial temperature distribution is shown in Fig. 2. The λ_e values were deduced by fitting the relationship between the measured temperatures and r using Eq. (1)) and they are summarized in Table 2. The deviation of the measured temperature from the calculated value was ±6% at a maximum. It was considered that the deviation was mainly caused by

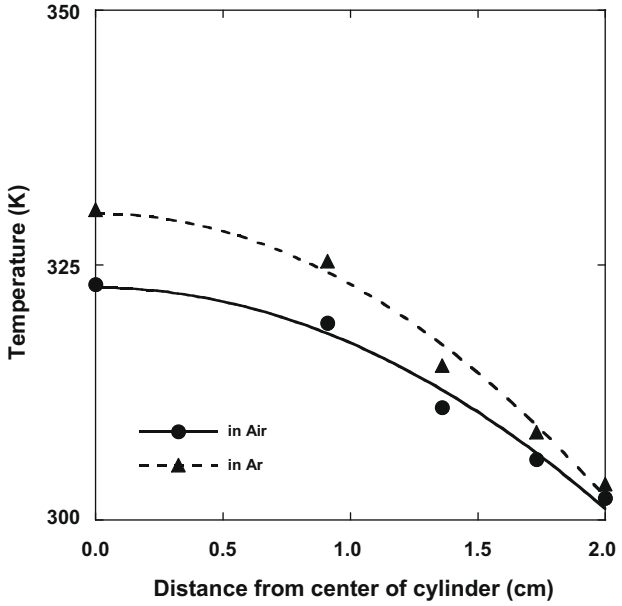

Fig. 2. Example of radial temperature distribution.

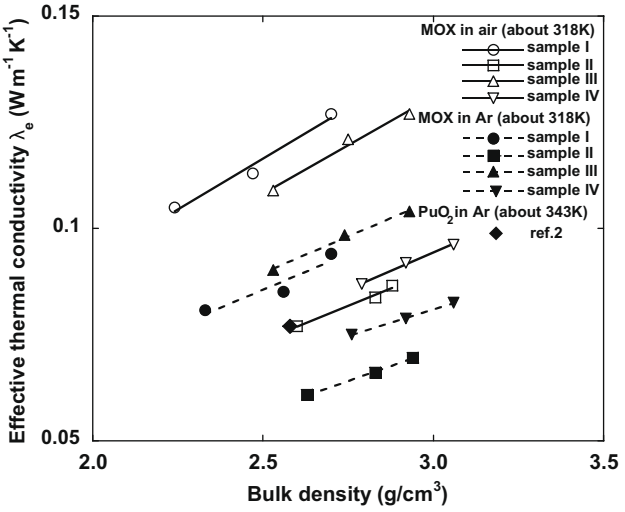

Fig. 3. Relation between bulk density and λ_e.

Table 2
Measurement conditions and effective thermal conductivity (λ_e).

Sample	Atmosphere	Bulk density (g/cm^3)	λ_e (W m^{-1} K^{-1})
I	Air	2.24	0.105
		2.47	0.113
		2.70	0.127
	Ar	2.33	0.0808
		2.56	0.0851
		2.70	0.094
II	Air	2.60	0.077
		2.83	0.0838
		2.88	0.0865
	Ar	2.63	0.0608
		2.83	0.0661
		2.94	0.0696
III	Air	2.53	0.109
		2.75	0.121
		2.93	0.127
	Ar	2.53	0.0902
		2.74	0.0985
		2.93	0.104
IV	Air	2.79	0.0869
		2.92	0.0919
		3.06	0.0962
	Ar	2.76	0.0750
		2.92	0.0788
		3.06	0.0825

the measuring error of the bulk density and the temperature detector position.

The λ_e values are plotted against the bulk density in Fig. 3. The measurements were carried out in air and Ar atmospheres, and the λ_e were in the range of 0.077–0.13 and in the range of 0.061–0.10 W m^{-1} K^{-1}, respectively. In previous work [2], the λ_e of plutonium oxide powder were measured, and the data was plotted in Fig. 3. The λ_e of plutonium oxide powder is consistent with those of MOX powder. The λ_e of MOX powder in air were higher than those in Ar, due to the difference of thermal conductivity of air (0.028 W m^{-1} K^{-1}, at 318 K) and Ar (0.019 W m^{-1} K^{-1}, at 318 K) [8]. The increase of the λ_e with the bulk density was caused by the decreasing volume fraction of the gas phase which had a lower thermal conductivity as compared with MOX particles. Samples I and III were observed to have larger λ_e as compared with samples II and IV. The difference between both was the O/M ratio as shown in Table 1.

4. Discussion

A number of tests have been carried out to investigate the thermal conductivity in discontinuous binary phases [3–6]. The bulk density of MOX raw powder is low value of 20–25%, and it is anticipated that thermal conductivity of interparticle is ignorable. Regarding the thermal conductivity of composite materials, Maxwell [3] investigated the effective thermal conductivity in discontinuous binary phases which included spherical particles of about 20 vol.%, and the model was as follows:

$$\lambda_e^* = \frac{2+\lambda_d^* - 2V_d(1-\lambda_d^*)}{2+\lambda_d^* + V_d(1-\lambda_d^*)}, \quad \lambda_e^* = \lambda_e/\lambda_c, \quad \lambda_d^* = \lambda_d/\lambda_c \tag{2}$$

where λ_e is effective thermal conductivity, λ_d is thermal conductivity of dispersed particles, λ_c is thermal conductivity of continuous phase and V_d is volume fraction of dispersed particles.

Later, Hamilton and Crosser [6] considered the effects of powder properties (such as mean particle size and specific surface area) and improved Maxwell's model as Eq. (2) as follows:

$$\lambda_e^* = \frac{\left(\frac{3}{\Psi^n}-1\right)+\lambda_d^* - \left(\frac{3}{\Psi^n}-1\right)V_d(1-\lambda_d^*)}{\left(\frac{3}{\Psi^n}-1\right)+\lambda_d^* + V_d(1-\lambda_d^*)} \tag{3}$$

where n is the constant of particle shape, $n = 1$ is sphere, $n = 1.5$ is oblate ellipsoid and $n = 2$ is a prolated ellipsoid. ψ is sphericity, and it is defined as the ratio of the surface area of a sphere, which has a volume equal to that of the particle, to the surface area of the particle.

In this work, the λ_e of MOX raw powder were evaluated by using the model of Hamilton and Crosser assuming that thermal conductivity of interparticle is ignorable. When density of dispersed particles is equal to theoretical density of MOX, ψ can be expressed as follows:

$$\Psi = \frac{4\pi(d/2)^2}{\rho_{th}\cdot\frac{4\pi}{3}(d/2)^3\cdot S} = \frac{6}{\rho_{th}\cdot d\cdot S} \tag{4}$$

where d is mean particle size of dispersed particles, ρ_{th} is theoretical density (11.18 g/cm^3), S is specific surface area of dispersed particles. In addition, V_d is defined as the ratio of bulk density to theoretical density.

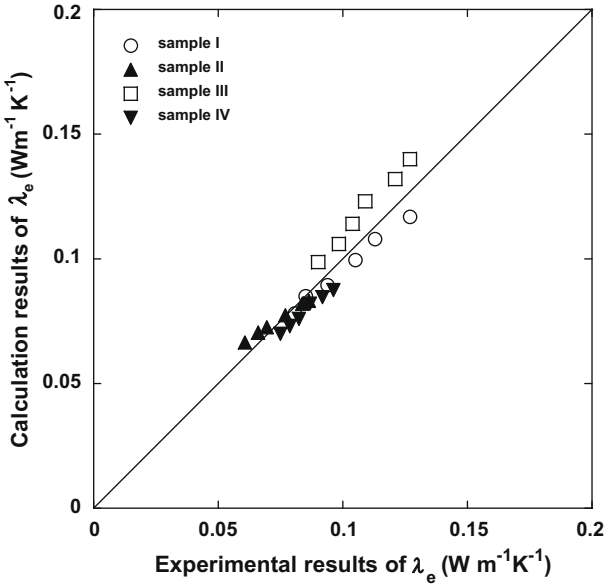

Fig. 4. Comparison between experimental and calculated results of λ_e.

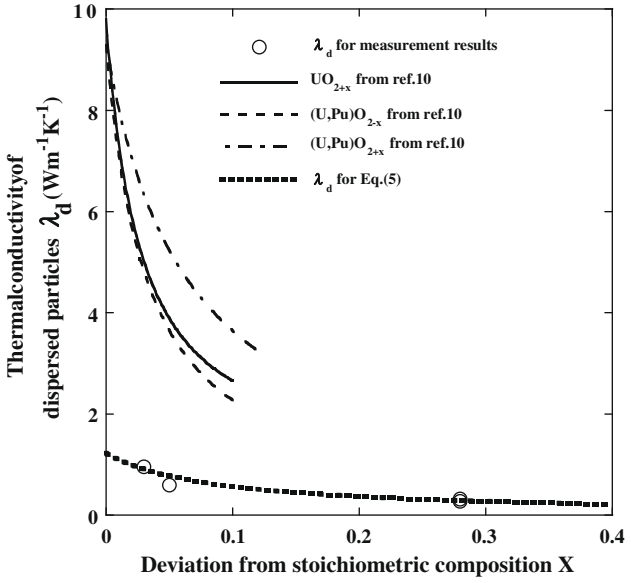

Fig. 5. Relation between O/M and λ_d.

The value of λ_d and n are unknown in Eqs. (2)–(4). So, λ_e^* was evaluated as a fitting parameter of λ_d and n. Fig. 4 compares experimental and calculated results of λ_e. In the case of $n = 1.7$ the calculated data reproduced the experimental data well with maximum error of ±11% as shown in the figure.

The evaluated λ_d are plotted in Fig. 5 as a function of O/M ratio; they decreased with the O/M ratio. In the oxide fuels, thermal conductivity by phonon conduction predominates at low temperature [9]. Thermal conductivities of UO_{2+X} and $(U,Pu)O_{2\pm X}$ have been reported [10,11]. Their data are also plotted in Fig. 5 for comparison. Thermal conductivity of UO_{2+X} decreased drastically with increasing deviation x from stoichiometric composition. The thermal conductivity of MOX also decreased. The thermal conductivity which was obtained in this work showed similar trends; however the

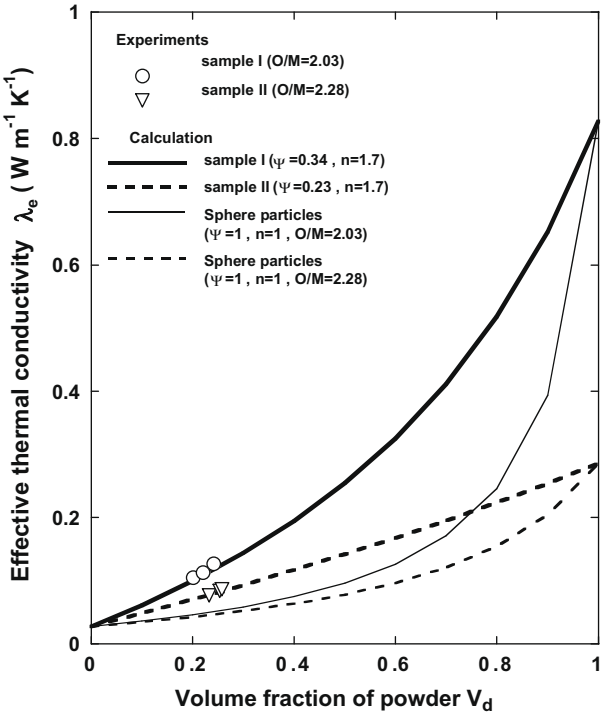

Fig. 6. Relation between V_d and λ_e.

thermal conductivity values were lower than literature data. This lower λ_d could be attributed to a large amount of defect concentration in the MOX raw powder. The relation between thermal conductivity of particles and O/M was obtained as shown in Eq. (5) assuming that λ_d was dominated by phonon conduction.

$$\lambda_d = \frac{1}{0.9331 + 9.171x} \tag{5}$$

where $0.9331 = 0.8906 + 1.336 \times 10^{-4} \times T$ ($T = 318$ K).

Fig. 6 shows the relation between V_d and λ_e in air, including the case of spherical particles (such as $n = 1$, $\psi = 1$). The calculated results of λ_e well accorded with experimental results. The λ_e varied significantly with V_d, λ_d and λ_c which were deduced from the bulk density, O/M ratio and kinds of gas, respectively. However, the increase of the bulk density caused the temperature increase due to the increase of the decay heat rate. Therefore, the use of gas having high λ_c and the adjustment of the O/M ratio to 2.00 were effective in controlling the powder temperature in the case of use of reactor-grade Pu.

5. Conclusion

The effective thermal conductivity was evaluated by measuring radial temperature distribution in MOX raw powder loaded into a cylindrical vessel. The effective thermal conductivity values in air and Ar were small, from 0.077 to 0.13 and 0.061 to 0.10 W m^{-1} K^{-1}, respectively. They changed significantly with O/M, bulk density and atmospheric gas.

The measurements in this work were analyzed using the model of Hamilton and Crosser, and the model to calculate the effective thermal conductivity for MH-MOX powder was derived as functions of powder properties, thermal conductivity of atmospheric gas and temperature. This derived model reproduced the experimental data with an error of ±11%.

Acknowledgements

The authors are pleased to acknowledge Mr H. Uno and Mr T. Tamura for their collaboration in the sample preparation.

References

[1] R. Eichler et al., J. Nucl. Mater. 124 (1984) 9.
[2] P. Bielenberg, Actinide Research Quarterly 3rd Quarter 2004 Actinide Oxides II, LALP-04-060, 2004, p. 18.
[3] J.C. Maxwell, A Treatise on Electricity and Magnetism, Oxford University Press, 1904. p. 435.
[4] H. Fricke, Phys. Rev. 24 (1924) 575.
[5] F.A. Johnson, Report of Atomic Energy Research Establishment, R/R2578, 1958.
[6] R.L. Hamilton, O.K. Crosser, I&EC Fundamentals, vol. 1(3), 1962. p. 187.
[7] US Department of Energy, Doe Standard, DOE-STD-1128-98, 1998.
[8] JSME Data Book, Heat Transfer, 3rd Ed., 1975, p. 300 (in Japanese).
[9] Y. Philipponneau, J. Nucl. Mater. 188 (1992) 194.
[10] D.G. Martin, J. Nucl. Mater. 110 (1982) 73.
[11] P.G. Lucuta et al., J. Nucl. Mater. 223 (1995) 51.